

Transport in strained graphene: Interplay of Abelian and axial magnetic fields

Aqeel Ahmed,^{1,2,*} Sanjib Kumar Das,^{2,*} and Bitan Roy²

¹*Department of Physics and Astronomy, Union College, Schenectady, New York, 12308, USA*

²*Department of Physics, Lehigh University, Bethlehem, Pennsylvania, 18015, USA*

(Dated: December 2, 2022)

Immersed in external magnetic fields, strained graphene constitutes an ideal tabletop setup, manifesting a confluence of Abelian (B) and axial (b) magnetic fields. In such a system, here we numerically compute two-terminal conductance (G), and four- as well as six-terminal Hall conductivity (σ_{xy}) for spinless fermions. In unstrained graphene ($b = 0$), the B -field produces quantized plateaus at $G = \pm|\sigma_{xy}| = (2n + 1)e^2/h$, where $n = 0, 1, 2, \dots$. Strain induced b -field lifts the two-fold valley degeneracy of higher Landau levels and leads to the formation of additional even integer plateaus at $G = \pm|\sigma_{xy}| = (2, 4, \dots)e^2/h$, when $B > b$. While the same sequence of plateaus is observed for G when $b > B$, any clear quantization of σ_{xy} in Hall bar geometries is absent due to numerical instability. A plateau at $G = \sigma_{xy} = 0$ always appears with the onset of a charge-density-wave order, causing a staggered pattern of fermionic density between two sublattices of honeycomb lattice.

Introduction. Interplay of Abelian (B) and axial (b) magnetic fields gives birth to a unique sequence of quantum Hall states and competing length scales of topological defect modes in two-dimensional Dirac materials [1–3]. In this regard, a honeycomb membrane of carbon atoms, graphene, constitutes a tabletop platform where such a confluence can be experimentally studied. When buckled, the electro-mechanical coupling in a graphene flake produces time-reversal symmetric axial magnetic fields [4–6]. Just like its Abelian counterpart, uniform axial magnetic fields produce valley degenerate Landau levels (LLs). While the real magnetic field points in the same direction near two inequivalent valleys of the erstwhile hexagonal Brillouin zone (BZ), harboring massless Dirac fermions, its axial cousin points in the opposite direction near the complementary valleys. Therefore, the net effective magnetic fields near two valleys are of different magnitude in the simultaneous presence of Abelian and axial fields. Moreover, their directions depend on the relative strengths of these two fields. Despite tremendous experimental activities exploring the quantum Hall physics in graphene over the past several years [7–12], the confluence of Abelian and axial magnetic fields has gained little experimental attention so far [13, 14].

Here we present a comprehensive numerical study of a mesoscopic graphene sample, subject to Abelian and/or axial magnetic fields in multi-terminal arrangements using Kwant [15]. Specifically, we compute two-terminal conductance (G) and transverse Hall conductivity (σ_{xy}) in four- and six-terminal setups [Fig. 1]. Throughout, G and σ_{xy} are measured in units of e^2/h . As the competition between the B and b fields is insensitive to electronic spin (leaving aside the Zeeman coupling of the former), here we consider a system of spinless fermions.

Key results. A flat graphene flake, subject to a real magnetic field (B), displays well-known quantized plateaus at $G = \pm|\sigma_{xy}| = 2n + 1$, manifesting the two-fold valley degeneracy of each LL, where $n = 0, 1, \dots$ [16] [Fig. 2]. A strain induced axial magnetic field (b) lifts the

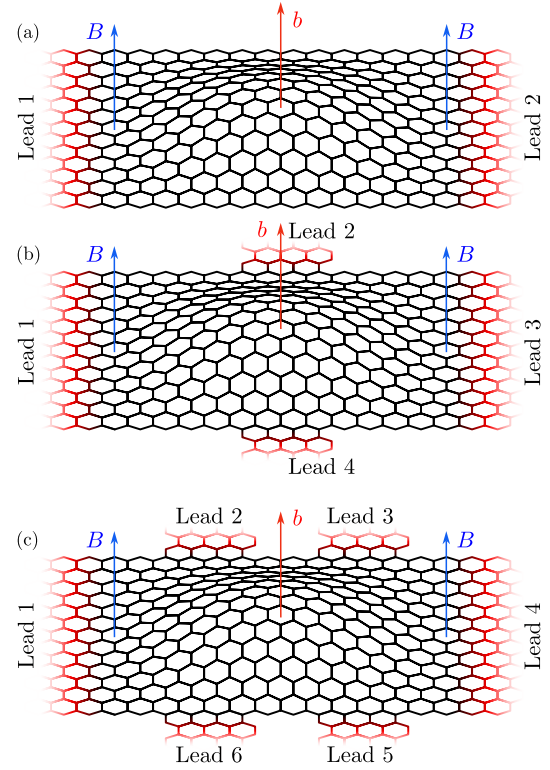


FIG. 1. Schematics of (a) two- (b) four- and (c) six-terminal setups. Semi-infinite red colored hexagons represent leads, attached to the scattering region (black) of length L and width W . The axial (b) [Abelian (B)] magnetic fields are shown by red [blue] arrows. Strain in graphene flake (producing b) is depicted by the bulge inside the scattering region.

valley degeneracy of all the LLs, except the topologically protected zeroth one [1, 2]. As a result when $B > b$, additional plateaus are observed at $G = \pm|\sigma_{xy}| = 2, 4, \dots$ [Fig. 3]. In the opposite limit when $b > B$, the higher LLs remain valley nondegenerate, and we find plateaus at $G = n + 1$. Once the real magnetic field is switched

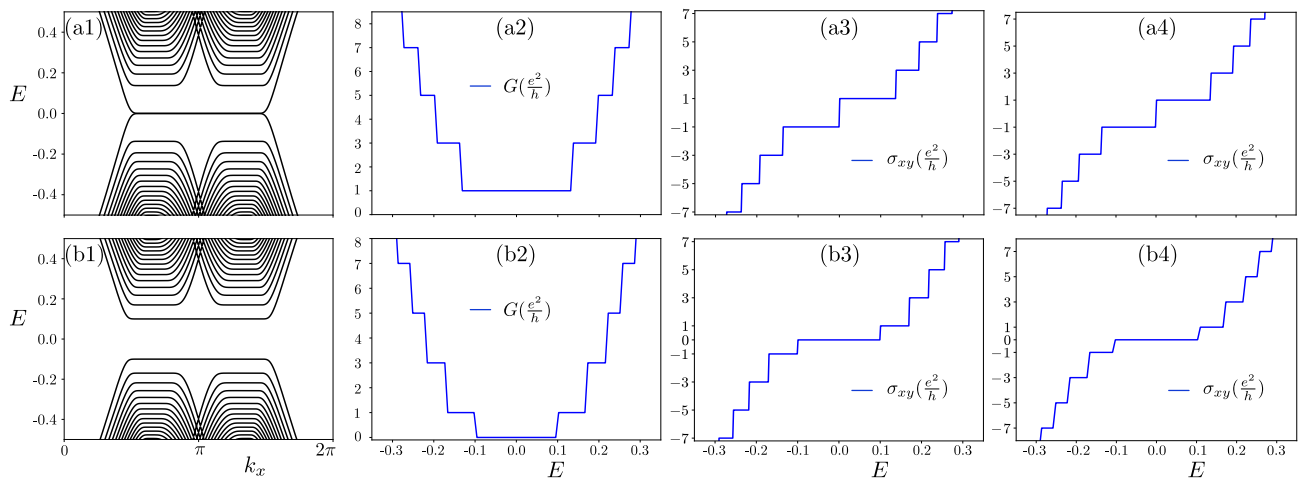


FIG. 2. Band structure of a zigzag graphene nanoribbon, containing 120 sites, for $t = 1$, $B = 2 \times 10^{-3}$, $\omega = 0.0$, and (a1) $\delta = 0.0$ and (b1) $\delta = 0.1$. The magnetic field induces flat two-fold valley degenerate electronlike and holelike LLs with energies $\sim \sqrt{n}$, where $n \in \mathbb{Z}$ is the LL index. Two-terminal conductance G , computed in a system of $L = W = 120$, shows quantized plateaus at $2n + 1$ in (a2) and (b2). The CDW order (δ) gives birth to the $G = 0$ conductance plateau in (b2), as it gaps out the zeroth LL. (a3) Four- and (a4) six-terminal Hall conductivities in a $L = W = 400$ system show quantized Hall plateaus at $\sigma_{xy} = \pm(2n + 1)$ when $\delta = 0$. A finite δ resolves the $\sigma_{xy} = 0$ Hall plateau in (b3) four- and (b4) six-terminal measurements. Here G and σ_{xy} are computed within the energy range $(-0.35, 0.35)$, containing 400 grid points.

off in an otherwise strained graphene, valley degenerate axial LLs lead to a plateau formation at $G = 2n + 1$, while $\sigma_{xy} = 0$. See Fig. 4. However, when the axial field dominates over a finite B field, the numerical procedure in four- and six-terminal geometries becomes unstable in Kwant, and we fail to capture any conclusive quantization of σ_{xy} . Formation of a charge-density-wave (CDW) order in all these cases gaps out the zeroth LL and in turn produces a $G = \sigma_{xy} = 0$ plateau [Figs. 2-4].

Model. The tight-binding Hamiltonian in graphene with only nearest-neighbor (NN) hopping (t_{jk}) reads as

$$H_0 = - \sum_{\langle j,k \rangle} t_{jk} a_j^\dagger b_k + H.c. . \quad (1)$$

The summation is restricted over three NN sites, and a_j^\dagger and a_j (b_j^\dagger and b_j) are the fermionic creation and annihilation operators on a (b) sublattices, respectively, constructed from the linear combinations of the Bravais vectors $\mathbf{a}_1 = (1, 0)d$ and $\mathbf{a}_2 = (1, \sqrt{3})d/2$. Throughout, we set the lattice spacing $d = 1$. A Fourier transformation of H_0 with $t_{jk} = t$, reveals linearly dispersing massless Dirac fermions near two inequivalent corners of the hexagonal BZ, suitably chosen at $\pm \mathbf{K} = 2\pi(\sqrt{3}, 1)/(\sqrt{3}d)$ [17]. The above model with only NN hopping belongs to class BDI and the zigzag edge of graphene hosts localized zero-energy topological modes [18].

The orbital effect of an external B field is incorporated via a Peierls substitution $t_{jk} \rightarrow t_{jk} \exp[2\pi i \phi_{jk}]$ [19]. The flux phase ϕ_{jk} is given by the line integral $\phi_{jk} = \int_j^k \mathbf{A} \cdot d\mathbf{l}$ from site j to site k . To introduce a uniform Abelian

magnetic field $\mathbf{B} = B\hat{z}$, we choose a Landau gauge for the magnetic vector potential $\mathbf{A} = (-By, 0, 0)$, such that $\nabla \times \mathbf{A} = \mathbf{B}$. It results in $t_{jk} \rightarrow t \exp[-i\pi\Phi(x_k - x_j)(y_j + y_k)]$, with $\Phi = Bel^2/h$ being the flux threading a unit cell of area l^2 . Here (x_j, y_j) is the real space coordinates of the site j [20]. Application of an external magnetic field quenches the conical Dirac dispersion into a set of highly degenerate LLs, as shown in Fig. 2(a1).

The axial or pseudo magnetic field in a graphene flake originates from a particular class of strain. For example, it can be modeled via a uniform modulation of one of the three NN bonds, here chosen to be the one perpendicular to the zigzag edge, from one end of the scattering region of width W to the other [21, 22]. The hopping amplitude along such bonds in the presence of Abelian and axial magnetic fields takes the form [2]

$$t_{jk} \rightarrow t \left[1 + \omega \frac{y_k}{W} \delta_{jk} \right] \exp[-i\pi\Phi(x_k - x_j)(y_j + y_k)], \quad (2)$$

where $y_k \in [-W, W]/2$, and the hopping along two other NN bonds retains its original strength t . Here ω measures the strength of the strain, yielding an axial magnetic field $b \sim \omega$. Due to the strain gradient, the axial LLs acquire slightly inhomogeneous Fermi velocity, and hence they are not perfectly flat. Compare Fig. 4(a) and Fig. 2(a1).

In half-filled graphene, the average fermionic density on any site is $1/2$. Maintaining the overall filling unchanged, the system can develop a staggered pattern of fermionic density between two sublattices, resulting in a CDW order. In the presence of Abelian and/or axial magnetic fields, it can be supported by sufficiently weak NN Coulomb repulsion, following the spirit of *magnetic*

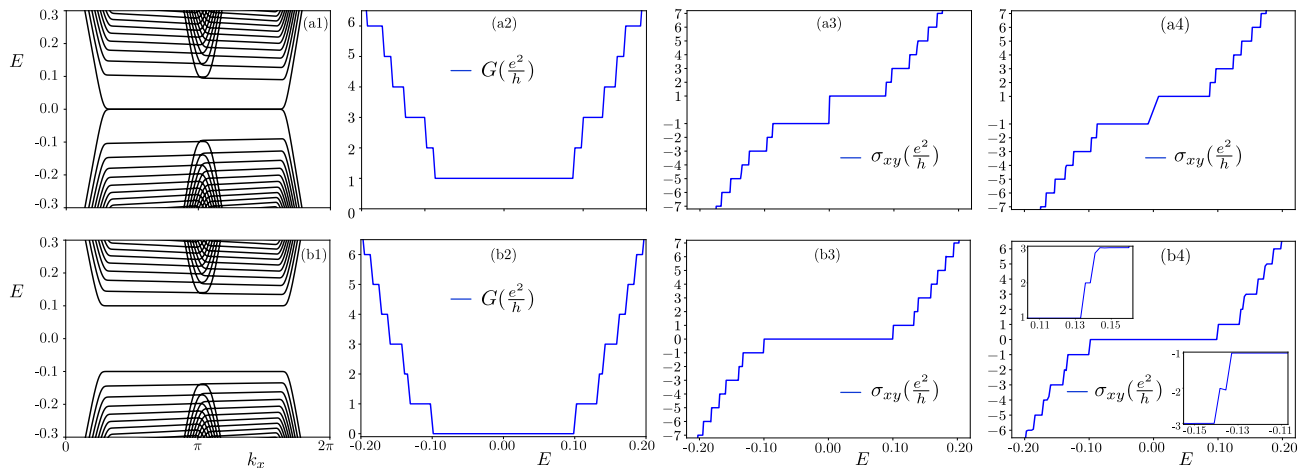


FIG. 3. Band structure of a zigzag graphene nanoribbon containing 400 sites for $B = 10^{-3}$, $\omega = 0.2$, such that $B > b$, and (a1) $\delta = 0.0$ and (b1) $\delta = 0.1$, for which two-terminal conductance is shown in (a2) and (b2), respectively. The Hall conductivity σ_{xy} in four- [six-] terminal setup is respectively shown in (a3) and (b3) [(a4) and (b4)]. Due to the valley degeneracy lifting of the higher LLs, additional even integer plateaus at $G = \pm|\sigma_{xy}| = 2, 4, \dots$ are formed (see Fig. 2), while the plateau at $G = \sigma_{xy} = 0$ appears only in the presence of the CDW order. Insets in (b4) shows the narrow plateaus for $\sigma_{xy} = \pm 2$. Numerical calculations are performed in a system with $L = W = 600$, and with 400 grid points in the energy window $(-0.25, 0.25)$.

catalysis [23–26]. Here, however, we add such an order from the outset, yielding average fermionic densities $1/2 \pm \delta$ on a and b sublattices, respectively. The quantity δ measures the strength of the CDW order. Next we discuss two-, four- and six-terminal setups to compute quantum transport in all these systems using Kwant [15].

Two-terminal transport. In a two-terminal setup, both the left and the right side of a square-shaped scattering region, made of graphene lattices, are connected to leads [Fig. 1(a)]. These symmetric leads are semi-infinite in the sense that they are connected to the system on one side and extend to infinity on the other side, preserving the translational invariance. In all our calculations, the leads and the scattering region have identical Hamiltonian. The leads are attached to all the last set of sites of the scattering region. The corresponding unitary scattering matrix is given by

$$S = \begin{pmatrix} r & t' \\ t & r' \end{pmatrix}, \quad (3)$$

preserving the total probability of the incoming and outgoing modes. Here r and r' (t and t') are the reflection (transmission) parts of S . We compute the conductance $G = \text{Tr}(t^\dagger t)$ of the system from the transmission channels. The trace (‘Tr’) is taken over the conducting channels. Notice that there is no bias voltage in the system.

Four-terminal transport. To capture the Hall response, one needs to go beyond the two-terminal arrangement, and consider a multi-terminal setup. Here we compute the four-terminal conductance in graphene, subject to real and/or pseudo magnetic fields. A current j flows between Lead 1 and Lead 3, and the Hall voltage develops between the vertical Lead 2 and Lead 4, acting as the

Hall probes [Fig. 1(b)]. Upon solving the current-voltage linear equation $\mathbf{j} = \mathbf{G}\mathbf{V}$, where \mathbf{G} is the 4×4 conductance matrix, we obtain the Hall voltage $V_2 - V_4$, where V_p is the voltage in the p th lead. The Hall conductivity in terms of $E_x = V_3 - V_1$ and $E_y = V_2 - V_4$ is given by

$$\sigma_{xy} = \frac{j_x E_y}{E_x^2 + E_y^2}. \quad (4)$$

In four-terminal setup, however, $E_x = 0$.

Six-terminal transport. Since the six-terminal Hall bar geometry is most commonly employed in experiments to measure Hall responses, here we also compute σ_{xy} in this setup [Fig. 1(c)]. It allows us to compute the transverse Hall voltage between two vertical leads [Lead 2 (3) and Lead 6 (5)] and a longitudinal voltage between Lead 5 (3) and Lead 6 (2). We consider a current j flowing only between Lead 1 and Lead 4 under the influence of an electric field \mathbf{E} . In the same spirit of the four-terminal calculation, here we have $E_x = V_2 - V_3$ and $E_y = V_3 - V_5$. Then σ_{xy} can be computed from Eq. (4). While computing σ_{xy} in Kwant, it is important to employ a fine energy mesh to observe its sharp quantized plateaus.

Results. To set the stage, we first consider a flat graphene, subject to Abelian magnetic fields (B). The system then supports two-fold valley degenerate flat LLs, resulting from bulk cyclotron orbits, at energies $\pm\sqrt{2nB}$. The two-terminal conductance then shows monotonically increasing *odd* integer quantized plateaus at $G = 2n + 1$, as the chemical potential is gradually tuned away from the half-filling, thereby enhancing the number of occupied unidirectional quantized transmission channels. However, this setup is insensitive to the direction of the

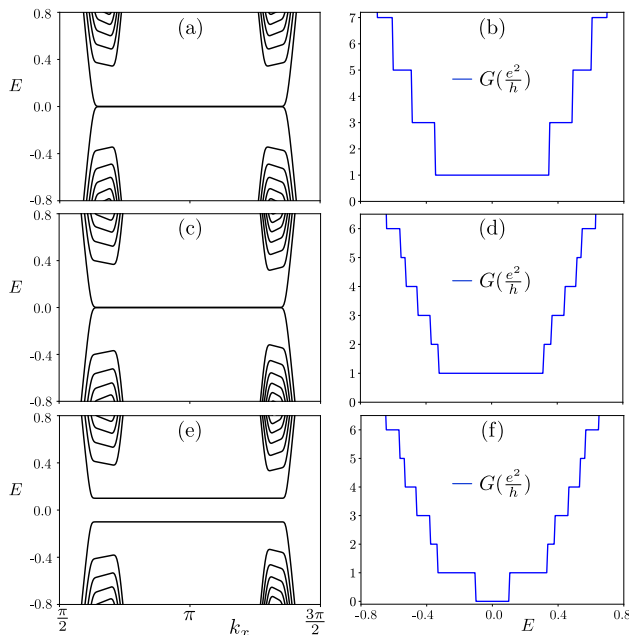


FIG. 4. Band structure of a zigzag graphene nanoribbon of 400 sites for $\omega = 0.3$, $B = 0$ [(a)] or $B = 2 \times 10^{-5}$ [(c) and (e)], and $\delta = 0.0$ [(a) and (c)] or $\delta = 0.1$ [(e)], such that $b > B$ (always), presented over a part of the BZ containing well-separated LLs, realized by setting $t = 10$. We compute two-terminal conductance (G) in a system with $L = W = 400$. (b) With $B = 0$, axial magnetic field (b) produces $G = 2n + 1$ plateaus, while additional even integer plateaus at $G = 2, 4, \dots$ appear with a finite but weak B -field in (d). (f) The CDW stabilizes the $G = 0$ plateau.

transmission channels and the nature of the carriers (electron or hole). Such a conundrum gets resolved in four- and six-terminal setups, both featuring quantized Hall conductivity plateaus at $\sigma_{xy} = \pm(2n + 1)$, respectively in the electron and hole doped regimes. The zeroth LLs near the opposite valleys live on complementary sublattices of graphene. Thus, formation of a CDW order gaps out the zeroth LL, thereby forming an insulator at half-filling. Then an additional plateau at $G = \sigma_{xy} = 0$ develops. These results are summarized in Fig. 2.

Once buckled, the resulting axial magnetic field (b) lifts the valley degeneracy of all the LLs, as the effective magnetic fields are now $\mathcal{B}_{\text{eff}}^{\pm} = (B \pm b)$ near the valleys at $\pm\mathbf{K}$, respectively. Two sets of particle-hole symmetric LLs then appear at energies $\pm[2n|\mathcal{B}_{\text{eff}}^{\pm}|]^{1/2}$ with the respective areal degeneracies $D_{\pm} = |\mathcal{B}_{\text{eff}}^{\pm}|/(2\pi)$. But, zeroth LLs remain pinned at zero energy, reflecting their topological protections [1, 2, 27]. Although it is challenging to extract b directly in terms of ω from Eq. (2), notice that when $B = b$, only one valley with $\mathcal{B}_{\text{eff}}^{+} = 2B = 2b$ hosts LLs, while the other one remains gapless as $\mathcal{B}_{\text{eff}}^{-} = 0$ therein. This is a quantum critical point, separating the field-dominated regime ($B > b$) from the strain dominated one ($b > B$). We first consider the former one [20].

When $B > b$, the edge modes for two copies of non-degenerate LLs propagate in the same direction, as the effective magnetic fields $\mathcal{B}_{\text{eff}}^{\pm} > 0$ point in the same direction near two valleys. Consequently, the two-terminal conductance shows plateaus at all integers. The Hall conductivity in a such system can be computed from the Středa formula $\sigma_{xy} = (\partial N/\partial B)_{\mu}$ [28]. Here N is the bulk electronic density and the derivative is taken at a fixed chemical potential (μ). Under a small change of the magnetic field δB , the change in the number of states below (for electron doping) or above (for hole doping) the chemical potential is $\delta N = \Omega(n_{+} + n_{-})\delta B$, where Ω is the area of the graphene sample and n_{\pm} is the number of filled LLs with areal degeneracies D_{\pm} , respectively, yielding $\sigma_{xy} = n_{+} + n_{-} = n$. Therefore, in the field dominated regime, the Hall conductivity only counts the number (n) of filled LLs at a fixed chemical potential, measured from the half-filling. Concomitantly, we find $\sigma_{xy} = \pm(n+1)$ in both four- and six-terminal Hall bar geometries. In this regime, zeroth LLs near two valleys continue to reside on complementary sublattices [1]. Thus, formation of a CDW order resolves an additional plateau at $G = \sigma_{xy} = 0$. These findings are displayed in Fig. 3.

Finally, we focus on the strain dominated regime, as pseudo or axial magnetic fields in buckled graphene can in principle be extremely large (a few hundred Tesla) [4–6]. When $B = 0$, the system supports valley degenerate axial LLs, which are, however, slightly dispersive, possibly stemming from a spatially modulated Fermi velocity of Dirac fermions. The edge modes, residing near the $\pm\mathbf{K}$ valleys propagate in the opposite directions, manifesting the time-reversal symmetry, and are thus helical. In such a system, we find $G = 2n + 1$ in a two-terminal setup as it only counts the number of conducting edge modes, while being insensitive to their helicity. This observation strongly promotes the topological nature of the helical edge modes, leading to quantized transport [Fig. 4]. But, $\sigma_{xy} = 0$ in both four- and six-terminal arrangements due to the preserved time-reversal symmetry [20].

Application of a weak external magnetic field ($B < b$), lifts the valley degeneracy of all the axial LLs, except the zeroth ones. We then find $G = n + 1$ [Fig. 4]. In this regime, the Středa formula implies $\sigma_{xy} = n_{+} - n_{-}$, suggesting an *oscillatory* behavior of the Hall conductivity as the chemical potential sweeps through the sea of electronlike or holelike LLs [2]. Unfortunately, the Kwant based numerical procedure in Hall bar geometries then becomes extremely unstable [20], possibly due to its gauge dependence in multi-terminal computation. And we fail to reach any conclusion on the quantization of σ_{xy} in the strain dominated regime. When $b > B$, the zeroth LL wavefunctions are localized on one sublattice near both valleys in the bulk of the system, while they live on the complementary sublattice near its boundary. Therefore, a CDW order can be developed by creating a density imbalance between the bulk and the boundary

of the system [26], which gaps out the zeroth LL and in turn stabilizes a plateau at $G = 0$ [Fig. 4].

Summary & discussions. Here we present lattice based extensive numerical analyses of quantum transport in strained graphene, immersed in external magnetic fields using Kwant [15], in two-, four-, and six-terminal arrangements, capturing hallmarks of the interplay between Abelian (B) and axial (b) magnetic fields [Fig. 1]. Our findings are consistent with theoretical predictions from the continuum model in various limits, which include (a) flat graphene in ordinary magnetic fields ($b = 0$) [Fig. 2] [16], (b) field dominated regime ($B > b$) [Fig. 3] [1], and (c) strain dominated regime (with only finite b as well as $b > B$) [Fig. 4] [2]. Possibly due to the explicit gauge dependence in the numerical procedure in Kwant, we failed to underpin the expected oscillatory behavior of σ_{xy} in the strain dominated regime [2]. To circumvent this limitation, we will reinvestigate this problem using nonequilibrium Green's function method in future [29, 30]. Furthermore, given that the thermal Hall conductivity (κ_{xy}) has been computed [31] and measured [32] in a flat graphene with B fields, in the future we will also compute quantized κ_{xy} , featuring the interplay of B and b fields. Our theoretical investigation should stimulate future experiments to showcase intriguing confluence of magnetic fields in two-dimensional Dirac materials, which is still in its infancy [13, 14].

Acknowledgments. S.K.D was supported by a Startup grant of B.R. from Lehigh University. A.A. was supported by the REU program through NSF-PHY 1852010. We thank Suvayu Ali for technical support.

* Equal contributors.

- [1] B. Roy, Odd integer quantum Hall effect in graphene, *Phys. Rev. B* **84**, 035458 (2011).
- [2] B. Roy, Z.-X. Hu, and K. Yang, Theory of unconventional quantum Hall effect in strained graphene, *Phys. Rev. B* **87**, 121408 (2013).
- [3] B. Roy, Magnetic-field induced inequivalent vortex zero modes in strained graphene, *Phys. Rev. B* **85**, 165453 (2012).
- [4] N. Levy, S. A. Burke, K. L. Meaker, M. Panlasigui, A. Zettl, F. Guinea, A. H. Castro Neto, and M. F. Crommie, Strain-Induced Pseudo-Magnetic Fields Greater Than 300 Tesla in Graphene Nanobubbles, *Science* **329**, 544 (2010).
- [5] K. K. Gomes, W. Mar, W. Ko, F. Guinea, and H. Manoharan, Designer Dirac fermions and topological phases in molecular graphene, *Nature (London)* **483**, 306 (2012).
- [6] J. Lu, A. H. Castro Neto, and K. P. Loh, Transforming moiré blisters into geometric graphene nano-bubbles, *Nat. Comm.* **3**, 823 (2012).
- [7] K. S. Novoselov, A. K. Geim, S. V. Morozov, D. Jiang, M. I. Katsnelson, I. V. Grigorieva, S. V. Dubonos, and A. A. Firsov, Two-dimensional gas of massless Dirac fermions in graphene, *Nature (London)* **438**, 197 (2005).
- [8] Y. Zhang, Y.-W. Tan, H. L. Stormer, and P. Kim, Experimental observation of the quantum Hall effect and Berry's phase in graphene, *Nature (London)* **438**, 201 (2005).
- [9] A. F. Young, C. R. Dean, L. Wang, H. Ren, P. Cadden-Zimansky, K. Watanabe, T. Taniguchi, J. Hone, K. L. Shepard, and P. Kim, Spin and valley quantum Hall ferromagnetism in graphene, *Nat. Phys.* **8**, 550 (2012).
- [10] B. E. Feldman, B. Krauss, J. H. Smet, and A. Yacoby, Unconventional Sequence of Fractional Quantum Hall States in Suspended Graphene, *Science* **337**, 1196 (2012).
- [11] G. L. Yu, R. Jalil, B. Belle, A. S. Mayorov, P. Blake, F. Schedin, S. V. Morozov, L. A. Ponomarenko, F. Chiappini, S. Wiedmann, U. Zeitler, M. I. Katsnelson, A. K. Geim, K. S. Novoselov, and D. C. Elias, Interaction phenomena in graphene seen through quantum capacitance, *Proc. Natl. Acad. Sci.* **110**, 3282 (2013).
- [12] H. Zhou, C. Huang, N. Wei, T. Taniguchi, K. Watanabe, M. P. Zaletel, Z. Papić, A. H. MacDonald, and A. F. Young, Strong-Magnetic-Field Magnon Transport in Monolayer Graphene, *Phys. Rev. X* **12**, 021060 (2022).
- [13] S.-Y. Li, K.-K. Bai, L.-J. Yin, J.-B. Qiao, W.-X. Wang, and L. He, Observation of unconventional splitting of Landau levels in strained graphene, *Phys. Rev. B* **92**, 245302 (2015).
- [14] S.-Y. Li, Y. Su, Y.-N. Ren, and L. He, Valley Polarization and Inversion in Strained Graphene via Pseudo-Landau Levels, Valley Splitting of Real Landau Levels, and Confined States, *Phys. Rev. Lett.* **124**, 106802 (2020).
- [15] C. W. Groth, M. Wimmer, A. R. Akhmerov, and X. Waintal, Kwant: a software package for quantum transport, *New J. Phys.* **16**, 063065 (2014).
- [16] V. P. Gusynin and S. G. Sharapov, Unconventional Integer Quantum Hall Effect in Graphene, *Phys. Rev. Lett.* **95**, 146801 (2005).
- [17] G. W. Semenoff, Condensed-Matter Simulation of a Three-Dimensional Anomaly, *Phys. Rev. Lett.* **53**, 2449 (1984).
- [18] M. Fujita, K. Wakabayashi, K. Nakada, and K. Kusakabe, Peculiar Localized State at Zigzag Graphite Edge, *J. Phys. Soc. Jpn.* **65**, 1920 (1996).
- [19] R. Peierls, Zur Theorie des Diamagnetismus von Leitungselektronen, *Z. Physik* **80**, 763 (1933).
- [20] See Supplemental Materials at XXX-XXXX for the details of Peierls phase computation, evolution of the LLs with B and b fields, and four-terminal σ_{xy} for $b > B$.
- [21] P. Ghaemi, J. Cayssol, D. N. Sheng, and A. Vishwanath, Fractional Topological Phases and Broken Time-Reversal Symmetry in Strained Graphene, *Phys. Rev. Lett.* **108**, 266801 (2012).
- [22] B. Roy and I. F. Herbut, Topological insulators in strained graphene at weak interaction, *Phys. Rev. B* **88**, 045425 (2013).
- [23] V. P. Gusynin, V. A. Miransky, S. G. Sharapov, and I. A. Shovkova, Excitonic gap, phase transition, and quantum Hall effect in graphene, *Phys. Rev. B* **74**, 195429 (2006).
- [24] I. F. Herbut, Theory of integer quantum Hall effect in graphene, *Phys. Rev. B* **75**, 165411 (2007).
- [25] B. Roy and I. F. Herbut, Inhomogeneous magnetic catalysis on graphene's honeycomb lattice, *Phys. Rev. B* **83**, 195422 (2011).
- [26] B. Roy and J. D. Sau, Competing charge-density wave, magnetic, and topological ground states at and near

- Dirac points in graphene in axial magnetic fields, *Phys. Rev. B* **90**, 075427 (2014).
- [27] Y. Aharonov and A. Casher, Ground state of a spin- $\frac{1}{2}$ charged particle in a two-dimensional magnetic field, *Phys. Rev. A* **19**, 2461 (1979).
- [28] P. Štředa, Theory of quantised hall conductivity in two dimensions, *J. Phys. C* **15**, L717 (1982).
- [29] D. H. Lee and J. D. Joannopoulos, Simple scheme for surface-band calculations. I, *Phys. Rev. B* **23**, 4988 (1981).
- [30] D. H. Lee and J. D. Joannopoulos, Simple scheme for surface-band calculations. II. The Green's function, *Phys. Rev. B* **23**, 4997 (1981).
- [31] W. Long, H. Zhang, and Q.-f. Sun, Quantum thermal Hall effect in graphene, *Phys. Rev. B* **84**, 075416 (2011).
- [32] S. K. Srivastav, M. R. Sahu, K. Watanabe, T. Taniguchi, S. Banerjee, and A. Das, Universal quantized thermal conductance in graphene, *Sci. Adv.* **5**, eaaw5798 (2019).